ActRIIB blockade increases force-generating capacity and preserves energy supply in exercising mdx mouse muscle in vivo

Nelly Béchir, Emilie Pecchi, Christophe Vilmen, Yann Le Fur, Helge Amthor, Monique Bernard, David Bendahan, Benoit Giannesini

ActRIIB blockade increases force-generating capacity and preserves energy supply in exercising mdx mouse muscle in vivo

Nelly Béchir[1], Emilie Pecchi[1], Christophe Vilmen[1], Yann Le Fur[1], Helge Amthor[2,3], Monique Bernard[1], David Bendahan[1], Benoît Giannesini[1]

[1] Aix-Marseille Université, CNRS, CRMBM UMR 7339, 13385, Marseille, France

[2] Université de Versailles Saint-Quentin-en-Yvelines, UFR des sciences de la santé, INSERM U1179, LIA BAHN CSM, SQY Therapeutics, 78180 Montigny-le-Bretonneux, France

[3] Service Génétique Médicale, CHU Necker-Enfants Malades, Université Paris Descartes, France

Correspondence should be addressed to:

Dr. Benoît GIANNESINI, PhD

Centre de Résonance Magnétique Biologique et Médicale (CRMBM)

UMR 7339 CNRS – Aix-Marseille Université

Faculté de Médecine de Marseille, 27 Bd Jean Moulin, 13385 Marseille

E-mail: benoit.giannesini@univ-amu.fr

Short title: Impact of ActRIIB blockade in dystrophic muscle

Abbreviations

^{31}P-MRS: 31-phosphorus MR spectroscopy

ActRIIB: activin type IIB receptor

DMD: Duchene muscular dystrophy

f_{50} : the electrostimulation frequency for which 50% of the maximal tension was exerted

MR: magnetic resonance

MHC: myosin heavy-chain

sActRIIB-Fc: soluble ActRIIB signaling inhibitor

τPCr_{rec}: time constant of phosphocreatine resynthesis during the post-exercise period

Abstract

Postnatal blockade of the activin type IIB receptor (ActRIIB) represents a promising therapeutic strategy for counteracting dystrophic muscle wasting. However, its impact upon muscle function and bioenergetics remains poorly documented under physiological condition. Here, we have investigated totally noninvasively the effect of 8-week administration of either soluble ActRIIB signaling inhibitor (sActRIIB-Fc) or vehicle PBS (control) on gastrocnemius muscle force-generating capacity, energy metabolism and anatomy in dystrophic mdx mice using magnetic resonance (MR) imaging and dynamic 31-phosphorus MR spectroscopy (^{31}P-MRS) in vivo. ActRIIB inhibition increased muscle volume (+33%) without changing fiber-type distribution, and increased basal animal oxygen consumption (+22%) and energy expenditure (+23%). During an in vivo standardized fatiguing exercise, maximal and total absolute contractile forces were larger (+40% and +24%, respectively) in sActRIIB-Fc treated animals, whereas specific force-generating capacity and fatigue resistance remain unaffected. Furthermore, sActRIIB-Fc administration did not alter metabolic fluxes, ATP homeostasis and contractile efficiency during the fatiguing bout of exercise, although it dramatically reduced the intrinsic mitochondrial capacity for producing ATP. Overall, sActRIIB-Fc treatment increased muscle mass and strength without altering the fundamental weakness characteristic of dystrophic mdx muscle. These data support the clinical interest of ActRIIB blockade for reversing dystrophic muscle wasting.

Keywords: Skeletal muscle hypertrophy; myostatin inhibition; Duchenne muscular dystrophy; muscle fatigue.

INTRODUCTION

ActRIIB is a transmembrane serine-threonine kinase receptor that mediates the signaling for myostatin (GDF8) and other members of the transforming growth factor β family involved in the negative regulation of skeletal muscle growth (1, 2). It has been shown that pharmaceutical disruption of ActRIIB signaling pathway using soluble ActRIIB receptor (sActRIIb-Fc) or neutralizing antibodies against ActRIIB or myostatin leads to a rapid and massive increase in muscle mass (3-9). These findings have put forward postnatal ActRIIB blockade as a promising strategy for reversing muscle wasting common to ageing (sarcopenia) and to muscle degenerative disorders such as Duchenne muscular dystrophy (DMD) (7, 10, 11).

DMD is a fatal X-linked myopathy caused by mutations in the DMD gene resulting in the absence or severe reduction of functional protein dystrophin from the sarcolemma (12). This disorder is characterized by muscle weakness in association with bioenergetics abnormalities including mitochondrial dysfunction and reduced basal content of high-energy phosphorylated compounds (13-15). Despite the molecular and pathophysiological mechanisms involved in DMD are well described, there is still no cure for restoring dystrophin. Then, stimulation of muscle growth throughout ActRIIB signaling disruption could be a mean for improving muscle function in DMD patient (16). Interestingly, in addition to the muscle mass growth, ActRIIB inhibition has been shown to reduce myofiber damage in response to contraction in the mdx mouse model of DMD (17, 18). However, the corresponding functional advantage remains poorly documented and controversial. For example, it has been reported in mdx mice that irrespectively of muscle typology, ActRIIB blockade either increases (3, 18), has no effect (19, 20) or even decreases (20) absolute force-generating capacity in electrostimulated muscle ex vivo. Moreover, considering that ActRIIB inhibition decreases fatigue resistance in healthy muscle (20, 21), sActRIIB-Fc treatment could be potentially deleterious for dystrophic muscle but this issue has never been addressed. At the bioenergetics level, indirect calorimetry experiments have

demonstrated that caloric output was increased by 25% in mdx mice treated with sActRIIb-Fc, hence suggesting that basal energy metabolism is disturbed (3). Furthermore, we and others have reported that the mRNA and protein levels of key regulatory genes promoting oxidative metabolism are reduced in mdx mice treated with soluble ActRIIB, which indicates that ActRIIB inhibition impairs oxidative muscle metabolism (20, 22). This impairment could have undesirable clinical consequences given that the dystrophic phenotype is by itself associated with mitochondrial dysfunction (14, 15) and low oxidative capacity is known to increase the risk for cardiovascular and metabolic diseases (23). Overall, it must be pointed out that the very few studies having investigating so far the effect of ActRIIB blockade upon dystrophic muscle function have been performed mainly in vitro, and data regarding mechanical performance in relation to energy production and regulation are then still missing.

The aim of this study was to determine the impact of ActRIIB inhibition on dystrophic muscle function and bioenergetics under physiological condition. For this purpose, mdx mice were injected semiweekly with the rodent form of sActRIIB-Fc for a total of 8 weeks. Gastrocnemius muscle force-generating capacity, energy metabolism and anatomy were investigated totally noninvasively using hindlimb MR imaging and ^{31}P-MRS as previously described (24). ^{31}P-MRS is a valuable technique for dynamically and simultaneously monitoring high-energy phosphorylated compounds levels, acidosis, oxidative capacity and ATP turnover in exercising muscle in vivo. We have analyzed the corresponding results together with lean mass and fat content quantification using whole-body MR imaging, indirect calorimetry measurements and fiber type composition determination from myosin heavy-chain (MHC) isoforms analysis.

MATERIALS AND METHODS

Animal care and feeding

Seventeen 3-month-old mdx mice generated from a colony maintained on a C57Bl/10ScSn background (Pierre et Marie Curie faculty of Medicine, Paris, France) were used for these experiments. All animal experiments were conducted in strict accordance with the guidelines of the European Communities Council Directive 86/609/EEC for Care and Use of Laboratory Animals, and were performed according to protocols reviewed and approved by the Institutional Animal Care Committee of Aix-Marseille University (permit number 93-21122012) under the supervision of BG (license number 13.164 2008/11/25). Every attempt was made to minimize the number and the suffering of animals. Mice were socially housed as 4-5 per cage in an environmentally controlled facility (12-12 h light-dark cycle, 22°C) with free access to commercial standard food and water. After experiments, animals were euthanized by cervical dislocation following isoflurane anesthesia. Gastrocnemius muscle were immediately removed, freeze-clamped with nitrogen-chilled metal tongs, and stored at -80°C for in vitro measurements.

Experimental design

In vivo blockade of ActRIIB signaling was done using a soluble fusion protein (sActRIIB-Fc, also called RAP-031, Acceleron Pharma Inc., Cambridge, MA, USA) generated by fusing the ActRIIB extracellular domain to the mouse immunoglobulin Fc region (5). Mice were randomly assigned to two groups and were injected subcutaneously twice weekly for a total of 8 weeks with sActRIIB-Fc (10 mg/kg body weight; n = 8) or an equal volume of vehicle (10 mM PBS; control group; n = 9).

Noninvasive investigation of gastrocnemius muscle function and energetics

Each animal was tested twice over a one-week period in order to evaluate totally noninvasively force-generating capacity, energy metabolism and anatomy in

electrostimulated gastrocnemius muscle. During the first testing session, hindlimb MR images were recorded to get information about muscle volume, and metabolic changes associated to muscle activity were investigated using ^{31}P-MR spectroscopy throughout a standardized fatiguing bout of exercise (6 min of repeated maximal isometric contractions induced electrically at a frequency of 1.7 Hz). During the second session, gastrocnemius muscle was electrostimulated with trains (0.75 sec duration; rest interval of 30 sec) of incremental frequencies (1, 10, 20, 30, 50, 75, 100, and 150 Hz) and the corresponding contractile tension was measured.

Animal preparation. Each mouse was initially anesthetized in an induction chamber using 4% isoflurane in 33% O_2 and 66% N_2O. The left hindlimb was shaved before electrode cream was applied at the knee and heel regions for optimizing transcutaneous muscle electrostimulation. Animal was then placed supine in a home-built cradle, which has been especially designed for the totally noninvasive MR investigation of gastrocnemius muscle function and bioenergetics (24); this muscle was chosen because it is easily accessible for MR measurements and preferentially activated using our experimental methods. The cradle integrates two rod-shaped transcutaneous electrodes (one electrode was located at the heel level and the other one was located above the knee joint) connected to a constant-current stimulator (DS7A; Digitimer, Herthfordshire, United Kingdom) and an ergometer consisting of a foot pedal coupled to a force transducer. This former was constructed by sticking a strain gauge (120-ohm internal resistance ref 1-LY11-6/120A; HBM GmbH, Darmstadt, Germany) on a 0.4-mm thickness Bakelite slat in a Wheatstone bridge design (3 × 120 ohm). Animal's foot was placed on the pedal of the ergometer and the hindlimb was centered inside a ^{1}H Helmholtz imaging coil (20-mm diameter) while the belly of the gastrocnemius muscle was positioned above an elliptic (8 x 12 mm^2) ^{31}P-MRS surface coil. Corneas were protected from drying by applying ophthalmic cream, and mouse's muzzle was placed in a facemask continuously supplied with 1.75% isoflurane in 33% O_2 (0.2 L/min) and 66% N_2O (0.4 L/min). Body temperature was controlled and maintained at a physiological level throughout the experiment using a feedback loop including an electrical heating blanket, a temperature

control unit (ref. 507137; Harvard Apparatus, Holliston, MA, USA) and a rectal thermometer constructed with a NTC thermistor SMC series (ref NCP18XW220J03RB-2.2K, Murata, Kyoto, Japan).

Mechanical data acquisition. Resting muscle was passively stretched by modifying the angle between the foot and the hindlimb in order to produce maximal isometric twitch tension in response to supramaximal square wave pulses (1-ms duration). The individual maximal electrostimulation intensity was determined by progressively increasing the stimulus intensity until there was no further peak twitch tension increase. Electrical signal coming out from the force transducer of the ergometer was amplified (Operational amplifier AD620; Analog Devices, Norwood, MA, USA; gain = 70 dB; 0-5 kHz bandwidth) and converted into a digital signal (PCI-6220; National Instrument, Austin, TX, USA) that was continuously monitored and recorded on a personal computer using the WinATS software version 6.5 (Sysma, Aix-en-Provence, France).

MR data acquisition. Explorations were performed in the 4.7-Tesla horizontal magnet of a 47/30 Biospec Avance MR system (Bruker, Karlsruhe, Germany) equipped with a 120-mm BGA12SL (200 mT/m) gradient insert. Ten consecutive noncontiguous axial slices (0.5-mm spaced; 1-mm thickness) covering the region from the knee to the ankle were selected across the hindlimb. RARE images of these slices (8 echoes; 67.9-ms effective echo time; 16.7-ms actual echo time; 2000-ms repetition time; one accumulation; 20 x 15 mm^2 field of view; 256 x 256 matrix size) were acquired at rest. ^{31}P-MR spectra (8 kHz sweep width; 2048 data points) from the gastrocnemius region were continuously recorded at rest (6 min), during the 6-min fatiguing bout of exercise, and during the following 15-min recovery period. MR data acquisition was gated to muscle electrostimulation for reducing potential motion artifacts due to contraction. A fully relaxed spectrum (12 scans, 20-s repetition time) was acquired at rest, followed by 768 free induction decays (FID; 1.875-s repetition time). The first 64 FIDs were acquired at rest and summed together. The next 192 FIDs were acquired during the fatiguing exercise and were summed by packets of 32, allowing a 60-s temporal resolution. The remaining 512 FIDs were obtained during the post-

electrostimulation recovery period and were summed as 7 packets of 32 FIDs followed by 3 packets of 64 FIDs and one packet of 96 FIDs.

Data processing. Mechanical data were processed as followed: For the fatiguing exercise, absolute force production (expressed as force-time integral, in N*s) was calculated by integrating the isometric force (in N) with respect to time. Specific force (in $N*s/mm^3$) was obtained by scaling absolute force to muscle volume calculated from hindlimb MR images (see below). For the incremental frequencies electrostimulation protocol, tension was measured for each train and the corresponding data were fitted to the Hill equation providing f_{50}, i.e., the stimulation frequency for which 50% of the maximal tension was exerted. MR data were processed with custom-written analysis algorithms developed using the IDL platform (Interactive Data Language, Research System, Inc., Boulder, CO, USA) (25, 26). Region of interest was manually outlined for each hindlimb MR image so that the corresponding cross sectional area of the gastrocnemius muscle was measured. Muscle volume was then calculated by summing the volumes included between consecutive slices. Relative concentrations of phosphocreatine (PCr), inorganic phosphate (P_i) and ATP were obtained from ^{31}P-MR spectra by a time-domain fitting routine using the AMARES-MRUI Fortran code (27) and appropriate prior knowledge for the ATP multiplets. Absolute concentrations were expressed relative to basal ATP level determined in vitro using a bioluminescence-based method (see below), and intracellular pH was calculated from the chemical shift of the P_i signal relative to PCr (28). ADP concentration was calculated from [PCr], [ATP] and pH considering the equilibrium constant (K = 1.67 10^9 M^{-1}) of the creatine kinase (CK) enzyme reaction (29).

Metabolic fluxes calculation. Metabolic fluxes from oxidative and anaerobic pathways were quantified during the 6-min fatiguing exercise as previously described (30-32). These robust and highly reproducible methods have been widely used to investigate muscle bioenergetics in vivo under physiological and pathological conditions in humans (33-35) and animal models (36-38). The rate of ATP production from oxidative phosphorylation (Q) was calculated considering that ADP stimulates mitochondrial ATP synthesis through a

hyperbolic relationship (39): $Q = Q_{max} / (1 + K_m / [ADP])$, where Q_{max} represents the maximal rate of oxidative ATP synthesis and K_m (i.e., ADP concentration at the half-maximal ATP oxidative rate) is approximately 30 μM in murine gastrocnemius muscle. Q_{max} was calculated as follows: $Q_{max} = VPCr_{rec} \times (1 + K_m / [ADP]_{end})$, where $VPCr_{rec}$ and $[ADP]_{end}$ is the initial rate of PCr resynthesis at the start of the recovery period and $[ADP]_{end}$ is the ADP level at the end of the fatiguing exercise. $VPCr_{rec}$ was the ratio between ΔPCr (the amount of PCr consumption measured at the end of the exercise) and τPCr_{rec} (the time constant of PCr resynthesis during the post-exercise period). In order to determine τPCr_{rec}, the time-course of the post-electrostimulation PCr resynthesis was fitted to a first-order exponential curve with a least mean-squared algorithm. Noteworthy, τPCr_{rec} is considered as an in vivo measure of the intrinsic mitochondrial oxidative capacity considering that PCr resynthesis during the postexercise recovery period relies exclusively on oxidative ATP generation (31, 40, 41).

Anaerobic ATP production rate was calculated as the sum between ATP produced by PCr degradation via CK reaction and by anaerobic glycolysis. The rate of ATP production from the CK reaction (D) was directly calculated using the time-course of PCr throughout the fatiguing exercise: $D = -dPCr/dt$. Glycolytic ATP production rate (L) was determined considering that it is related to glycolytic proton generation (H_{Gly}) with a stoichiometry of 1.5 moles ATP per mole of proton (42): $L = 1.5 \times H_{Gly}$. Proton generation can be inferred from intramuscular pH taking into account (i) protons consumed by PCr degradation via the CK reaction (H_{CK}), (ii) protons passively buffered in the muscle cytosol (H_β), (iii) proton efflux from the cell (H_{Efflux}) and (iv) protons produced by oxidative phosphorylation (H_{Ox}): $H_{Gly} = H_{CK} + H_\beta + H_{Efflux} - H_{Ox}$ (32). H_{CK} was calculated from the time-dependent changes in [PCr] using the proton stoichiometric coefficient ($\varphi = 1 / (1 + 10^{(pH-6.75)})$ representing the number of protons generated per mole of PCr degraded (43): $H_{CK} = \varphi dPCr/dt$. The amount of protons buffered in the cytosol was estimated from the apparent buffering capacity (β_{total}, in Slykes, millimoles acid added per unit change in pH) and from the rate of pH change: $H_\beta = -\beta_{total} \times dpH/dt$, where β_{total} takes into account the buffering capacity of P_i ($\beta_{Pi} = 2.3[P_i] / ((1+10^{(pH-}$

$^{6.75)}$)(1+10$^{(6.75-pH)}$)) and the tissue buffering capacity (β_{tissue}) (43). It has been shown that β_{tissue} varies linearly between pH 7 (16 Slykes) and pH 6 (37 Slykes) in murine gastrocnemius muscle (44); accordingly, β_{tissue} = -21pH + 123. Proton efflux was calculated using the linear pH-dependence constant (λ, in mM/min/pH unit) relating proton efflux rate and pH: H_{efflux} = -$\lambda\Delta$pH. The constant λ was determined from the initial recovery after electrostimulation cessation and considering that, despite the intracellular proton load associated with aerobic PCr resynthesis, pH recovers back to its basal value as a result of a net proton efflux from the cell: λ = -H_{efflux} / ΔpH. Therefore, H_{efflux} can be calculated considering proton production from CK reaction and mitochondrial ATP synthesis and pH changes: H_{efflux} = H_{CK} + H_{Ox} +β_{total}dpH/dt. Proton production by oxidative ATP synthesis was quantified from the coefficient m, which represents the number of proton produced by mole of ATP generated through oxidative phosphorylation (43): H_{Ox} = mVPCr$_{rec}$, with m = 0.16 / (1 + 10$^{(6.1-pH)}$).

In vivo quantification of body fat content

MRI acquisitions were performed with the 47/30 Biospec Avance MR system, using a whole-body imaging coil (PRK 200 RES 200, Bruker, Karlsruhe, Germany). Mice were anesthetized with isoflurane as described above. Axial MR images were acquired across the entire body length excluding the tail using a high-resolution 3-D (turbo spin echo) sequence (5.530-ms echo time; 77.85-ms effective echo time; 300-ms repetition time; 2 averages; 40 x 40 x 80 mm^3 field of view, 128 x 128 x 64 matrix size). Fat volume was quantified using an automatic segmentation method based on a pixel intensity analysis of MR images with FSL (FMRIB Software Library v5.0.2.2, Oxford University, UK; http://www.fmrib.ox.ac.uk/fsl). Fat mass was calculated considering that density of adipose tissue is 0.92 g/cm^3 (45).

Indirect calorimetry measurements

Measurements were performed using a two-chamber Oxylet system (Panlab, Barcelona, Spain) with a constant inlet flow of room air (5 mL/min) maintained throughout the

experiment. The temperature of the calorimetric room was set at 23°C. Animals were individually acclimated and kept for 24 h in metabolic cages with free access to food and water. Total oxygen consumption (VO_2) and CO_2 production (VCO_2) were continuously analyzed with the following sequence: 5 min from cage #1, 5 min from cage #2, and 5 min from room air. Energy expenditure (EE) was calculated as follows: EE = VO_2 x (3.815 + 1.232RQ), where RQ is the respiratory ratio of VCO_2 to VO_2. Ambulatory activity was determined simultaneously with the collection of indirect calorimetry data.

Myosin heavy-chain (MHC) isoforms analysis

Freeze-clamped muscles (50 mg) were homogenized in 600 µl of a solution containing 300 mM NaCl, 100 mM NaH_2PO_4, 50 mM Na_2HPO_4, 10 mM $Na_4P_2O_7$ 10, 1 mM $MgCl_2$, 10 mM EDTA and 1.4 mM β-mercaptoethanol, pH 6.5. After incubation (24 h at 4°C), the homogenates were centrifuged (15 min, 13000 x *g*, 4°C) and the supernatants were diluted 1:1 with glycerol. Total protein concentrations were measured with the Pierce BCA Protein Assay Kit (Thermo Scientific, Illkirch, France) according to manufacturer's instructions. Two µg of total proteins were denatured and run on 8% polyacrylamide gels for 48 h at 72 V using a Mini Protean Tetra system (Bio-Rad, Marnes-la-Coquette, France) (46). Gels were then stained with IRDye® Blue Protein Stain (LI-COR Biosciences, Lincoln, NE, USA) and scanned (42-µm spatial resolution) in the 700-nm channel of an infrared imaging system (Odyssey®, LI-COR Biosciences, Lincoln, NE, USA). MHC isoforms were identified according to their apparent molecular masses and quantified using the ImageJ software (http://imagej.nih.gov/ij/).

In vitro determination of intramuscular ATP content

Freeze-clamped muscles (40-60 mg) were homogenized in 1.2 mL of ice-cold perchloric acid (0.6 M). After incubation (15 min at 4°C), homogenates were centrifuged (15 min, 2000 x *g*, 4°C), and the supernatants were neutralized with K_2CO_3 and placed for 30 min at 4°C. ATP concentrations were determined using the Bioluminescence ATP

Determination Kit (ref. A22066, Invitrogen, Eugene, OR, USA). Luminescence was measured on a micro-plate reader (Victor X3, PerkinElmer, Waltham, MA, USA). All samples were run in duplicate.

Statistical analysis

All data are reported as means ± SEM. Body weight differences were evaluated by two-factor (group × time) analysis of variance (ANOVAs) with repeated measures on time followed when appropriate by Tukey-Kramer post-hoc multiple comparison tests for determining pairwise differences between groups. Other differences were determined by paired or unpaired two-tailed Student's *t*-test. The significance level was set at $P < 0.05$. All analyses were performed with JMP software version 9 (SAS Institute Inc., Cary, NC, USA).

RESULTS

Physiological changes

Mice treated with sActRIIB-Fc displayed a large and continuous increase in body weight (**Fig. 1a**). They were significantly heavier than PBS-treated animals one week after initiation of injections and until the end of the 8-week treatment period (**Fig. 1a**). At that time, food intake, body weight and lean mass were larger (+18%, +22% and +25%, respectively) in the group treated with sActRIIB-Fc (**Figs. 1b,c,d**), whereas fat mass did not differ between both groups (**Fig. 1e**). Further, sActRIIB-Fc led to a dramatic increase (+33%) in gastrocnemius muscle volume (**Fig. 1f**), but did not affect the relative distribution of MHC isoform proteins (**Figs. 1g,h**).

Indirect calorimetry measurements

Treatment with sActRIIB-Fc increased both oxygen consumption and energy expenditure (+22% and +23%, respectively; **Figs. 2a,b**) whereas the respiratory ratio (**Fig. 2c**) and the ambulatory activity (**Fig. 2d**) did not differ between both groups.

Gastrocnemius muscle mechanical performance

The force-frequency curve was constructed from contractile force data obtained during gastrocnemius muscle electrostimulation with trains of incremental frequencies (**Fig. 3a**). Single twitch tension was 32% larger in animals treated with sActRIIB-Fc (**Fig. 3b**), whereas maximal tetanic force and f_{50} (the electrostimulation frequency for which 50% of the maximal force was exerted) were not affected by sActRIIB-Fc treatment (**Fig. 3c,d**). Changes in absolute contractile force throughout the 6-min in vivo fatiguing bout of exercise were similar between both groups (**Fig. 4a**): force transiently increased in the early stage of the exercise to reach a maximal value that was 40% larger in animals receiving sActRIIB-Fc (**Fig. 4b**). Afterward, force progressively decreased as a sign of fatigue development until the end of the exercise; at this stage, the extent of force reduction did not differ between both groups (**Fig. 4c**). Overall, total force produced during the whole exercise was 24% larger in animals receiving sActRIIB-Fc (**Fig. 4d**). Besides, the shape of specific force curve during the fatiguing exercise was similar between PBS and sActRIIB-Fc groups (**Fig. 5a**). Noteworthy, maximal (**Fig. 5b**) and total specific force produced during the whole exercise (**Fig. 5c**) were not altered by sActRIIB-Fc treatment.

Bioenergetics, metabolic fluxes and energy cost of contraction

Bioenergetics variables were assessed in vivo throughout a standardized rest-exercise-recovery protocol. In resting muscle, PCr content was significantly larger (+20%) in animals treated with sActRIIB-Fc (**Table 1**). On the contrary, there were no difference between groups for [PCr]/[ATP], [ATP], [P_i] and pH. During the 6-min fatiguing exercise, PCr was initially degraded at a rate that was 73% larger in sActRIIB-Fc-treated animals (**Table**

1). After 3 min, PCr stabilized until the cessation of contractions (**Fig. 6a**) hence indicating the establishment of a metabolic steady state. At that time, the extent of PCr degradation was 35% larger in sActRIIB-Fc group (**Table 1**), thereby revealing that the energetics stress in response to exercise was higher in these mice. In both groups, P_i accumulated throughout the exercise with an initial phase of rapid and massive accumulation followed by a phase of steady state (**Fig. 6b**), whereas ATP level remained close to the basal value during the whole exercise (**Fig. 6c**), which indicates that ATP homeostasis was maintained. Importantly, the fact that the extent of ATP depletion at the end of the exercise did not differ between both groups (**Table 1**) led to assume that ATP regeneration capacity was not altered in sActRIIB-Fc treated mice. Intracellular acidosis is contracting muscle is mainly due to ATP production from glycolysis (42). In the present study, the time-course of intracellular pH was characterized by a rapid acidosis in the first half of the exercise (**Fig. 6d**), thereby indicating an acceleration of the glycolytic flux. After 3 min of exercise, pH reached a steady state in PBS-controls mice and remained fairly constant until the cessation of contractions; in the sActRIIB-Fc treated group on the contrary, pH decreased continuously until the end of the exercise (**Fig. 6d**) when it reached a value that was lower than in the PBS group (**Table 1**). Over the whole exercise, it is noteworthy that sActRIIB-Fc treatment did not affect oxidative, anaerobic and total ATP production (**Figs. 7a-c**). Also, there were no differences between groups for the relative contribution of oxidative and anaerobic processes to ATP production (**Fig. 7d**) and for ATP cost of contraction (**Fig. 7e**). During the recovery period following the fatiguing exercise, phosphorylated compound levels and pH progressively reached their respective basal values (**Figs. 6a-d**). Noteworthy, sActRIIB-Fc treatment prolonged (+60%) the PCr resynthesis time constant (τPCr_{rec}), thereby demonstrating a reduced intrinsic mitochondrial oxidative capacity (31, 40, 41). Nevertheless, there were no differences between both groups for the initial rates of PCr resynthesis ($VPCr_{rec}$) and proton efflux (**Table 1**).

DISCUSSION

This is the first in vivo study investigating the effect of long-term pharmaceutical ActRIIB blockade on dystrophic skeletal muscle function and bioenergetics. The key findings are that sActRIIB-Fc administration: (i) promotes gastrocnemius muscle volume without altering the relative distribution of MHC isoforms; (ii) increases both maximal and total absolute contractile forces produced throughout a fatiguing bout of exercise, whereas specific force-generating capacity and fatigue resistance are not disturbed; (iii) does not affect metabolic fluxes, ATP homeostasis and energy cost of contraction in contracting muscle, but (iv) prolongs the time constant of oxidative PCr resynthesis following muscle activity. At the whole-body level, ActRIIB blockade further increases lean mass, oxygen consumption and energy expenditure, but has no effect on body fat content and respiratory ratio.

As expected, long-term ActRIIB inhibition led to dramatic morphological changes. At the end of the 8-week treatment period, body weight and gastrocnemius muscle volume were larger (+22% and +33%, respectively) in mice receiving sActRIIB-Fc. The fact that the extent of muscle mass gain was larger than that of body weight augmentation could be linked to a greater effect of ActRIIB inhibition on lean mass as already observed in myostatin-deficient animals (2, 47) and in wild-type mice treated with sActRIIB-Fc (48). Actually, we have evidenced using whole-body MR imaging that sActRIIB-Fc treatment significantly increased lean mass but had no effect on body fat content, hence suggesting that ActRIIB inhibition alters basal energy homeostasis. We have performed indirect calorimetry experiments to test this assumption and found that ActRIIB inhibition increased both animal oxygen consumption and energy expenditure (+22% and +23%, respectively) while the ambulatory activity remained unchanged. These findings, which are comparable to those from previous studies in hypertrophied myostatin-deficient mice (47, 49), demonstrate that sActRIIB-Fc treatment increases the basal metabolic rate, which could ultimately affect animal endurance capacity. Also, it must be underlined that the treatment did not alter the

respiratory ratio thereby indicating that the relative contributions of lipid oxidation and carbohydrate to basal energy demand remained unchanged. Importantly, the fact that ActRIIB inhibition increased lean mass without affecting body fat content is in line with the view that hypertrophied muscle favors dietary fat utilization for growth and maintenance, which in return limits adipose tissue accumulation (50).

A major step was to determine in vivo whether ActRIIB blockade is beneficial for dystrophic muscle mechanical performance. We found that single maximal twitch tension (+32%) and total absolute force production during the fatiguing bout of exercise (+24%) were larger in hypertrophic gastrocnemius muscle, which is consistent with another study showing that ActRIIB blocking induces a roughly proportional increase in body mass and grip strength in mdx mice (51). Also, we did not detect any difference between both groups for maximal and total specific forces produced during the whole fatiguing exercise. These data corroborate ex vivo experiments in extensor digitorum longus muscle from sActRIIB-Fc treated mdx mice (3, 17, 18) and further evidence that muscle capacity for generating force takes full advantage of muscle hypertrophy. Noteworthy, lack of dystrophin leads to repeated cycles of fiber degeneration and regeneration processes that decrease the sarcolemma integrity with age so that muscle becomes more susceptible to contraction-induced injury. Then, it would be of interest to further determine whether the larger maximal force-generating capacity we measured in sActRIIB-Fc treated mdx mice is maintained with age. To a larger extent, given that high levels of mechanical stress are known to produce muscle damage in patients with DMD (52), one can wonder whether these patients could fully benefit from potent improved maximal force capacity resulting from the ActRIIB blockade or whether this would exacerbate the disease.

Moreover, the present study constitutes the first demonstration that sActRIIB-Fc treatment does not affect fatigue resistance in dystrophic muscle despite an increased fatigability has already been shown in hypertrophied muscle of myostatin-deficient mice (53, 54). In these mice, the larger fatigability has been attributed to typological changes with a shift toward glycolytic fibers, which are poorly resistant to fatigue. In accordance with

previous measurements of fiber-type distribution in soleus and extensor digitorum longus muscles from wild-type and mdx mice submitted to ActRIIB inhibition (20, 55), we found that sActRIIB-Fc treatment did not disturb gastrocnemius muscle typology, which could explain why muscle fatigability was not altered in mdx mice submitted to ActRIIB blockade. This finding stands out from our calorimetry experiments data suggesting that soluble ActRIIB treatment alters animal endurance capacity. Nevertheless, on must be aware that we have tested fatigue resistance during short duration standardized exercise and the effect of soluble ActRIIB treatment on endurance capacity warrants to be further investigated throughout prolonged exercise session.

Surprisingly, we observed that ActRIIB blockade did not improve maximal tetanic tension whereas it increased single twitch tension. These results are however in no way unusual since similar observations have been reported in isolated muscles from animals lacking myostatin (56) or mice treated with sActRIIB-Fc (21, 48) or myostatin neutralizing antibodies (9). The underlying cause for this phenomenon remains to be elucidated. It is unlikely that this is due to any decreased myofilaments sensitivity to calcium because we found that the stimulation frequency for which 50% of the maximal force was exerted – an in vivo indicator of calcium sensitivity (57) – was not affected by sActRIIB-Fc treatment. On the other hand, it is established that myostatin deficiency reduces muscle collagen content, thereby altering muscle mechanistic by increasing the stiffness of muscle aponevrosis and tendon (58, 59). It is then conceivable herein that long-term ActRIIB blockade produces similar alterations hence reducing the ability to generate tetanic tension because of limitation of individual twitches fusion during high-frequency repetitive stimulations.

Another important result is that sActRIIB-Fc treatment produced marked alterations in dystrophic muscle bioenergetics. First and foremost, we measured that ActRIIB blockade dramatically increased (+60%) the time constant of PCr resynthesis following repeated fatiguing contractions similarly to what has been already reported in ^{31}P-MRS studies in animals lacking myostatin (60) and in wild-type and dystrophic mice treated with soluble ActRIIB (20). Such an increase indicates that the intrinsic mitochondrial capacity for

generating ATP was reduced (31, 40, 41), which corroborates in vitro experiments demonstrating that mRNA and protein levels of key regulatory genes promoting oxidative metabolism are reduced in mdx mice treated with soluble ActRIIB (20, 22) and therefore joints the view that ActRIIB inhibition is deleterious for mitochondrial function (20, 22, 61). In addition, we found that sActRIIB-Fc treatment increased the basal PCr content, accelerated the start-exercise PCr degradation rate and worsened both acidosis and PCr depletion during sustained muscle activity. It must be kept in mind that PCr is under the control of the creatine kinase (CK) enzyme reaction to play a critical role in muscle bioenergetics. The PCr-CK system indeed acts to maintain ATP pool highly charged in exercising muscle, functioning as an energy buffer at the transition from rest to exercise and afterwards as an energy carrier directly involved in the transport of high-energy phosphate between mitochondria and the sites of ATP utilization (myofilaments and ion pumps). Thus, it is tempting to hypothesize that the metabolic alterations induced by sActRIIB treatment compromises energy supply in contracting muscle. However, this hypothesis can be ruled out here since there were no differences between both groups for oxidative and anaerobic ATP production fluxes during exercise. As a result, we found that sActRIIB-Fc treatment did not disturb ATP homeostasis in exercising muscle, which means that ATP regeneration entirely fitted ATP demand for contraction. Moreover, despite the reduced intrinsic mitochondrial capacity for generating ATP, we found that sActRIIB-Fc treatment did not affect $V\text{PCr}_{rec}$, i.e., the apparent oxidative capacity. $V\text{PCr}_{rec}$ was calculated as the ratio between ΔPCr (the amount of PCr consumption measured at the end of the exercise) and the postexercise PCr resynthesis time constant (31, 40, 41). Consequently, the larger basal PCr content in sActRIIB-Fc treated animals could be interpreted as a compensatory mechanism allowing a “normal” apparent oxidative capacity in the face of the intrinsic mitochondrial failure. Besides, we found that the ATP cost of contraction, which reflects the contractile efficiency, was not altered by sActRIIB-Fc treatment. This result might appear at a first glance paradoxical with the increased energy expenditure we have characterized using calorimetric experiments in awaked animals treated with sActRIIB-Fc. However, it must be

kept in mind that this increase was measured at rest at the whole-body level and might then differ from what is measured in exercising muscle.

In conclusion, this study provides original data demonstrating that ActRIIB signaling plays a crucial role in whole-body mass control, muscle function and bioenergetics in mdx mice. Given that ActRIIB signaling endows muscle with higher oxidative capacity and fatigue resistance (20, 54), the risk was that ActRIIB inhibition exacerbates the dystrophic phenotype, which is by itself already associated with mitochondrial dysfunction and impaired muscle mechanical performance (14, 15). Yet, we found that although it dramatically reduces the intrinsic mitochondrial capacity for producing ATP, sActRIIB-Fc treatment does not alter metabolic fluxes, ATP homeostasis and contractile efficiency during a fatiguing bout of exercise, and further increases muscle mass and strength. Our findings therefore support the potential clinical interest of ActRIIB blockade for reversing dystrophic muscle wasting.

ACKNOWLEDGEMENTS

We are grateful to Acceleron Pharma Inc. for the gift of sActRIIB-Fc. The authors also thank Ms Laurence Louis (Plate-Forme Génomique et Transcriptomique, Aix-Marseille Université, INSERM, UMR S910, Marseille, France) for helpful assistance with infrared imaging, and Dr Delphine Bastelica and Dr Marie-Christine Alessi (NORT, Aix-Marseille Université, INSERM U1062/INRA 1260, Marseille, France) for sharing the indirect calorimetry system. This work was financially supported by the French Muscular Dystrophy Association (AFM-Téléthon).

GRANTS

This work was financially supported by the French Muscular Dystrophy Association (AFM-Téléthon).

DISCLOSURE

The authors have no conflicts of interest, financial or otherwise, to declare. Acceleron Pharma Inc. did not influence data collection, analysis, interpretation and decision to publish the present study.

REFERENCES

1. De Caestecker, M. (2004) The transforming growth factor-beta superfamily of receptors. *Cytokine Growth Factor Rev* **15**, 1-11
2. Lee, S. J., and McPherron, A. C. (2001) Regulation of myostatin activity and muscle growth. *Proc Natl Acad Sci USA* **98**, 9306-9311
3. Bogdanovich, S., Krag, T. O., Barton, E. R., Morris, L. D., Whittemore, L. A., Ahima, R. S., and Khurana, T. S. (2002) Functional improvement of dystrophic muscle by myostatin blockade. *Nature* **420**, 418-421
4. Wang, Q., and McPherron, A. C. (2012) Myostatin inhibition induces muscle fibre hypertrophy prior to satellite cell activation. *J Physiol (Lond)* **590**, 2151-2165
5. Morrison, B. M., Lachey, J. L., Warsing, L. C., Ting, B. L., Pullen, A. E., Underwood, K. W., Kumar, R., Sako, D., Grinberg, A., Wong, V., Colantuoni, E., Seehra, J. S., and Wagner, K. R. (2009) A soluble activin type IIB receptor improves function in a mouse model of amyotrophic lateral sclerosis. *Exp Neurol* **217**, 258-268
6. Attie, K. M., Borgstein, N. G., Yang, Y., Condon, C. H., Wilson, D. M., Pearsall, A. E., Kumar, R., Willins, D. A., Seehra, J. S., and Sherman, M. L. (2013) A single ascending-dose study of muscle regulator ACE-031 in healthy volunteers. *Muscle Nerve* **47**, 416-423
7. Lee, S. J., Reed, L. A., Davies, M. V., Girgenrath, S., Goad, M. E., Tomkinson, K. N., Wright, J. F., Barker, C., Ehrmantraut, G., Holmstrom, J., Trowell, B., Gertz, B., Jiang, M. S., Sebald, S. M., Matzuk, M., Li, E., Liang, L. F., Quattlebaum, E., Stotish, R. L., and Wolfman, N. M. (2005) Regulation of muscle growth by multiple ligands signaling through activin type II receptors. *Proc Natl Acad Sci USA* **102**, 18117-18122
8. Lach-Trifilieff, E., Minetti, G. C., Sheppard, K., Ibebunjo, C., Feige, J. N., Hartmann, S., Brachat, S., Rivet, H., Koelbing, C., Morvan, F., Hatakeyama, S., and Glass, D. J.

(2014) An antibody blocking activin type II receptors induces strong skeletal muscle hypertrophy and protects from atrophy. *Mol Cell Biol* **34**, 606-618

9. LeBrasseur, N. K., Schelhorn, T. M., Bernardo, B. L., Cosgrove, P. G., Loria, P. M., and Brown, T. A. (2009) Myostatin inhibition enhances the effects of exercise on performance and metabolic outcomes in aged mice. *J Gerontol A Biol Sci Med Sci* **64**, 940-948
10. Lawlor, M. W., Read, B. P., Edelstein, R., Yang, N., Pierson, C. R., Stein, M. J., Wermer-Colan, A., Buj-Bello, A., Lachey, J. L., Seehra, J. S., and Beggs, A. H. (2011) Inhibition of activin receptor type IIB increases strength and lifespan in myotubularin-deficient mice. *Am J Pathol* **178**, 784-793
11. Dumonceaux, J., and Amthor, H. (2009) Current advances in the development of therapies for neuromuscular disorders based on myostatin signalling, 3rd International Institute of Myology Workshop, Paris, September 12th, 2008. *Neuromuscul Disord* **19**, 797-799
12. Hoffman, E. P., Brown, R. H., Jr., and Kunkel, L. M. (1987) Dystrophin: the protein product of the Duchenne muscular dystrophy locus. *Cell* **51**, 919-928
13. Cole, M. A., Rafael, J. A., Taylor, D. J., Lodi, R., Davies, K. E., and Styles, P. (2002) A quantitative study of bioenergetics in skeletal muscle lacking utrophin and dystrophin. *Neuromuscul Disord* **12**, 247-257
14. Rybalka, E., Timpani, C. A., Cooke, M. B., Williams, A. D., and Hayes, A. (2014) Defects in mitochondrial ATP synthesis in dystrophin-deficient mdx skeletal muscles may be caused by complex I insufficiency. *PLoS One* **9**, e115763
15. Godin, R., Daussin, F., Matecki, S., Li, T., Petrof, B. J., and Burelle, Y. (2012) Peroxisome proliferator-activated receptor gamma coactivator1- gene alpha transfer restores mitochondrial biomass and improves mitochondrial calcium handling in post-necrotic mdx mouse skeletal muscle. *J Physiol (Lond)* **590**, 5487-5502

16. Amthor, H., and Hoogaars, W. M. (2012) Interference with myostatin/ActRIIB signaling as a therapeutic strategy for Duchenne muscular dystrophy. *Curr Gene Ther* **12**, 245-259

17. Bogdanovich, S., Perkins, K. J., Krag, T. O., Whittemore, L. A., and Khurana, T. S. (2005) Myostatin propeptide-mediated amelioration of dystrophic pathophysiology. *Faseb J* **19**, 543-549

18. Pistilli, E. E., Bogdanovich, S., Goncalves, M. D., Ahima, R. S., Lachey, J., Seehra, J., and Khurana, T. (2011) Targeting the activin type IIB receptor to improve muscle mass and function in the mdx mouse model of Duchenne muscular dystrophy. *Am J Pathol* **178**, 1287-1297

19. Morine, K. J., Bish, L. T., Selsby, J. T., Gazzara, J. A., Pendrak, K., Sleeper, M. M., Barton, E. R., Lee, S. J., and Sweeney, H. L. (2010) Activin IIB receptor blockade attenuates dystrophic pathology in a mouse model of Duchenne muscular dystrophy. *Muscle Nerve* **42**, 722-730

20. Relizani, K., Mouisel, E., Giannesini, B., Hourde, C., Patel, K., Morales Gonzalez, S., Julich, K., Vignaud, A., Pietri-Rouxel, F., Fortin, D., Garcia, L., Blot, S., Ritvos, O., Bendahan, D., Ferry, A., Ventura-Clapier, R., Schuelke, M., and Amthor, H. (2014) Blockade of ActRIIB signaling triggers muscle fatigability and metabolic myopathy. *Mol Ther* **22**, 1423-1433

21. Chiu, C. S., Peekhaus, N., Weber, H., Adamski, S., Murray, E. M., Zhang, H. Z., Zhao, J. Z., Ernst, R., Lineberger, J., Huang, L., Hampton, R., Arnold, B. A., Vitelli, S., Hamuro, L., Wang, W. R., Wei, N., Dillon, G. M., Miao, J., Alves, S. E., Glantschnig, H., Wang, F., and Wilkinson, H. A. (2013) Increased muscle force production and bone mineral density in ActRIIB-Fc-treated mature rodents. *J Gerontol A Biol Sci Med Sci* **68**, 1181-1192

22. Rahimov, F., King, O. D., Warsing, L. C., Powell, R. E., Emerson, C. P., Jr., Kunkel, L. M., and Wagner, K. R. (2011) Gene expression profiling of skeletal muscles treated with a soluble activin type IIB receptor. *Physiol Genomics* **43**, 398-407

23. Wisloff, U., Najjar, S. M., Ellingsen, O., Haram, P. M., Swoap, S., Al-Share, Q., Fernstrom, M., Rezaei, K., Lee, S. J., Koch, L. G., and Britton, S. L. (2005) Cardiovascular risk factors emerge after artificial selection for low aerobic capacity. *Science* **307**, 418-420

24. Giannesini, B., Vilmen, C., Le Fur, Y., Dalmasso, C., Cozzone, P. J., and Bendahan, D. (2010) A strictly noninvasive MR setup dedicated to longitudinal studies of mechanical performance, bioenergetics, anatomy, and muscle recruitment in contracting mouse skeletal muscle. *Magn Reson Med* **64**, 262-270

25. Mattei, J. P., Fur, Y. L., Cuge, N., Guis, S., Cozzone, P. J., and Bendahan, D. (2006) Segmentation of fascias, fat and muscle from magnetic resonance images in humans: the DISPIMAG software. *Magma* **19**, 275-279

26. Le Fur, Y., Nicoli, F., Guye, M., Confort-Gouny, S., Cozzone, P. J., and Kober, F. (2010) Grid-free interactive and automated data processing for MR chemical shift imaging data. *Magma* **23**, 23-30

27. Vanhamme, L., van den Boogaart, A., and Van Huffel, S. (1997) Improved method for accurate and efficient quantification of MRS data with use of prior knowledge. *J Magn Reson* **129**, 35-43

28. Arnold, D. L., Bore, P. J., Radda, G. K., Styles, P., and Taylor, D. J. (1984) Excessive intracellular acidosis of skeletal muscle on exercise in a patient with a post-viral exhaustion/fatigue syndrome. A 31P nuclear magnetic resonance study. *Lancet* **1**, 1367-1369

29. Roth, K., and Weiner, M. W. (1991) Determination of cytosolic ADP and AMP concentrations and the free energy of ATP hydrolysis in human muscle and brain tissues with 31P NMR spectroscopy. *Magn Reson Med* **22**, 505-511

30. Conley, K. E., Blei, M. L., Richards, T. L., Kushmerick, M. J., and Jubrias, S. A. (1997) Activation of glycolysis in human muscle in vivo. *Am J Physiol* **273**, C306-315

31. Kemp, G. J., Ahmad, R. E., Nicolay, K., and Prompers, J. J. (2015) Quantification of skeletal muscle mitochondrial function by 31P magnetic resonance spectroscopy techniques: a quantitative review. *Acta Physiol (Oxf)* **213**, 107-144

32. Kemp, G. J., and Radda, G. K. (1994) Quantitative interpretation of bioenergetic data from ^{31}P and ^{1}H magnetic resonance spectroscopic studies of skeletal muscle: an analytical review. *Magn Reson Q* **10**, 43-63

33. Amara, C. E., Shankland, E. G., Jubrias, S. A., Marcinek, D. J., Kushmerick, M. J., and Conley, K. E. (2007) Mild mitochondrial uncoupling impacts cellular aging in human muscles in vivo. *Proc Natl Acad Sci USA* **104**, 1057-1062

34. Conley, K. E., Kushmerick, M. J., and Jubrias, S. A. (1998) Glycolysis is independent of oxygenation state in stimulated human skeletal muscle in vivo. *J Physiol (Lond)* **511**, 935-945

35. Erkintalo, M., Bendahan, D., Mattei, J. P., Fabreguettes, C., Vague, P., and Cozzone, P. J. (1998) Reduced metabolic efficiency of skeletal muscle energetics in hyperthyroid patients evidenced quantitatively by in vivo phosphorus-31 magnetic resonance spectroscopy. *Metabolism* **47**, 769-776.

36. Kemp, G. J., Sanderson, A. L., Thompson, C. H., and Radda, G. K. (1996) Regulation of oxidative and glycogenolytic ATP synthesis in exercising rat skeletal muscle studied by ^{31}P magnetic resonance spectroscopy. *NMR Biomed.* **9**, 261-270

37. Giannesini, B., Izquierdo, M., Le Fur, Y., Cozzone, P. J., and Bendahan, D. (2001) In vivo reduction in ATP cost of contraction is not related to fatigue level in stimulated rat gastrocnemius muscle. *J Physiol (Lond)* **536**, 905-915

38. Macia, M., Pecchi, E., Vilmen, C., Desrois, M., Lan, C., Portha, B., Bernard, M., Bendahan, D., and Giannesini, B. (2015) Insulin Resistance Is Not Associated with an Impaired Mitochondrial Function in Contracting Gastrocnemius Muscle of Goto-Kakizaki Diabetic Rats In Vivo. *PLoS One* **10**, e0129579

39. Gyulai, L., Roth, Z., Leigh, J. S., Jr., and Chance, B. (1985) Bioenergetic studies of mitochondrial oxidative phosphorylation using 31phosphorus NMR. *J Biol Chem* **260**, 3947-3954

40. Arnold, D. L., Matthews, P. M., and Radda, G. K. (1984) Metabolic recovery after exercise and the assessment of mitochondrial function in vivo in human skeletal muscle by means of ^{31}P NMR. *Magn Reson Med* **1**, 307-315

41. Lanza, I. R., Bhagra, S., Nair, K. S., and Port, J. D. (2011) Measurement of human skeletal muscle oxidative capacity by 31P-MR spectroscopy: a cross-validation with in vitro measurements. *J Magn Reson Imaging* **34**, 1143-1150

42. Hochachka, P. W., and Mommsen, T. P. (1983) Protons and anaerobiosis. *Science* **219**, 1391-1397

43. Wolfe, C. L., Gilbert, H. F., Brindle, K. M., and Radda, G. K. (1988) Determination of buffering capacity of rat myocardium during ischemia. *Biochim Biophys Acta* **971**, 9-20

44. Adams, G. R., Foley, J. M., and Meyer, R. A. (1990) Muscle buffer capacity estimated from pH changes during rest-to-work transitions. *J Appl Physiol* **69**, 968-972

45. Farvid, M. S., Ng, T. W., Chan, D. C., Barrett, P. H., and Watts, G. F. (2005) Association of adiponectin and resistin with adipose tissue compartments, insulin resistance and dyslipidaemia. *Diabetes Obes Metab* **7**, 406-413

46. Birot, O. J., Koulmann, N., Peinnequin, A., and Bigard, X. A. (2003) Exercise-induced expression of vascular endothelial growth factor mRNA in rat skeletal muscle is dependent on fibre type. *J Physiol (Lond)* **552**, 213-221

47. McPherron, A. C., and Lee, S. J. (2002) Suppression of body fat accumulation in myostatin-deficient mice. *J Clin Invest* **109**, 595-601

48. Akpan, I., Goncalves, M. D., Dhir, R., Yin, X., Pistilli, E. E., Bogdanovich, S., Khurana, T. S., Ucran, J., Lachey, J., and Ahima, R. S. (2009) The effects of a soluble activin type IIB receptor on obesity and insulin sensitivity. *Int J Obes (Lond)* **33**, 1265-1273

49. Guo, T., Jou, W., Chanturiya, T., Portas, J., Gavrilova, O., and McPherron, A. C. (2009) Myostatin inhibition in muscle, but not adipose tissue, decreases fat mass and improves insulin sensitivity. *PLoS One* **4**, e4937

50. Zhao, B., Wall, R. J., and Yang, J. (2005) Transgenic expression of myostatin propeptide prevents diet-induced obesity and insulin resistance. *Biochem Biophys Res Commun* **337**, 248-255

51. George Carlson, C., Bruemmer, K., Sesti, J., Stefanski, C., Curtis, H., Ucran, J., Lachey, J., and Seehra, J. S. (2011) Soluble activin receptor type IIB increases forward pulling tension in the mdx mouse. *Muscle Nerve* **43**, 694-699

52. Petrof, B. J. (1998) The molecular basis of activity-induced muscle injury in Duchenne muscular dystrophy. *Mol Cell Biochem* **179**, 111-123

53. Giannesini, B., Vilmen, C., Amthor, H., Bernard, M., and Bendahan, D. (2013) Lack of myostatin impairs mechanical performance and ATP cost of contraction in exercising mouse gastrocnemius muscle in vivo. *Am J Physiol Endocrinol Metab* **305**, E33-40

54. Mouisel, E., Relizani, K., Mille-Hamard, L., Denis, R., Hourde, C., Agbulut, O., Patel, K., Arandel, L., Morales-Gonzalez, S., Vignaud, A., Garcia, L., Ferry, A., Luquet, S., Billat, V., Ventura-Clapier, R., Schuelke, M., and Amthor, H. (2014) Myostatin is a key mediator between energy metabolism and endurance capacity of skeletal muscle. *Am J Physiol Regul Integr Comp Physiol* **307**, R444-454

55. Cadena, S. M., Tomkinson, K. N., Monnell, T. E., Spaits, M. S., Kumar, R., Underwood, K. W., Pearsall, R. S., and Lachey, J. L. (2010) Administration of a soluble activin type IIB receptor promotes skeletal muscle growth independent of fiber type. *J Appl Physiol (1985)* **109**, 635-642

56. Amthor, H., Macharia, R., Navarrete, R., Schuelke, M., Brown, S. C., Otto, A., Voit, T., Muntoni, F., Vrbova, G., Partridge, T., Zammit, P., Bunger, L., and Patel, K. (2007) Lack of myostatin results in excessive muscle growth but impaired force generation. *Proc Natl Acad Sci USA* **104**, 1835-1840

57. Russ, D. W., Ruggeri, R. G., and Thomas, J. S. (2009) Central activation and force-frequency responses of the lumbar extensor muscles. *Med Sci Sports Exerc* **41**, 1504-1509

58. Mendias, C. L., Marcin, J. E., Calerdon, D. R., and Faulkner, J. A. (2006) Contractile properties of EDL and soleus muscles of myostatin-deficient mice. *J Appl Physiol* **101**, 898-905

59. Welle, S., Cardillo, A., Zanche, M., and Tawil, R. (2009) Skeletal muscle gene expression after myostatin knockout in mature mice. *Physiol Genomics* **38**, 342-350

60. Baligand, C., Gilson, H., Menard, J. C., Schakman, O., Wary, C., Thissen, J. P., and Carlier, P. G. (2009) Functional assessment of skeletal muscle in intact mice lacking myostatin by concurrent NMR imaging and spectroscopy. *Gene Ther* **17**, 328-337

61. Zhao, B., Li, E. J., Wall, R. J., and Yang, J. (2009) Coordinated patterns of gene expressions for adult muscle build-up in transgenic mice expressing myostatin propeptide. *BMC Genomics* **10**, 305

Table 1

Effect of 8-week treatment with PBS or sActRIIB-Fc on gastrocnemius muscle bioenergetics assessed in vivo using ^{31}P-MRS.

	PBS	sActRIIB-Fc
Resting period		
[PCr]/[ATP]	2.95 ± 0.13	3.22 ± 0.16
[PCr], mM	9.9 ± 0.4	11.9 ± 0.6*
[ATP], mM	3.4 ± 0.2	3.8 ± 0.3
[P_i], mM	1.2 ± 0.2	1.3 ± 0.2
pH	7.16 ± 0.04	7.11 ± 0.02
Onset of the 6-min fatiguing exercise		
Initial rate of PCr consumption, mM/min	6.0 ± 0.8	10.4 ± 1.0*
End of the 6-min fatiguing exercise		
PCr depletion (relative to rest), mM	7.4 ± 0.3	10.0 ± 0.4*
ATP depletion (relative to rest), mM	0.15 ± 0.22	0.70 ± 0.35
pH	6.66 ± 0.02	6.45 ± 0.05*
Post-exercise recovery period		
PCr resynthesis time constant (τPCr_{rec}), min	2.3 ± 0.3	3.7 ± 0.4*
Initial rate of PCr resynthesis ($VPCr_{rec}$), mM/min	2.8 ± 0.4	2.0 ± 0.3
Proton efflux, mM/min	1.8 ± 1.3	1.9 ± 1.8

Data are means ± SEM. * Significantly different from PBS.

FIGURE LEGENDS

Figure 1: Physiological changes. Changes in body weight throughout a 8-week treatment with PBS or sActRIIB-Fc in mdx mice (**a**). Daily food intake (b), body weight (**c**), lean (**d**) and fat mass (**e**), gastrocnemius muscle volume (**f**) and MHC isoform proteins (**g**) at the end of the treatment. Representative blot depicting the electrophoretic separation of MHC isoform (**h**). Data are means ± SEM. * Significantly different from PBS.

Figure 2: Indirect calorimetry measurements. Effect of a 8-week treatment with PBS or sActRIIB-Fc on oxygen consumption (**a**), energy expenditure (**b**), respiratory quotient (**c**) and ambulatory activity (**d**) in awaked mdx mice over a 24-hour period in individual calorimetric cages. Data are means ± SEM. * Significantly different from PBS.

Figure 3: Force frequency relationship in gastrocnemius muscle. Absolute contractile tension produced by the gastrocnemius muscle during the in vivo force-frequency protocol (**a**). Treatment with sActRIIB-Fc increased single twitch tension (**b**) but has no effect on maximal tetanic force (**c**) and f_{50} (**d**), which is the electrostimulation frequency for which 50% of the maximal isometric tension was exerted. Data are means ± SEM. * Significantly different from PBS.

Figure 4: Gastrocnemius muscle absolute force-generating capacity. Absolute force produced throughout the 6-min in vivo fatiguing exercise performed simultaneously to the dynamic ^{31}P-MRS acquisition after a 8-week treatment with PBS or sActRIIB-Fc (**a**). Maximal force (**b**), extent of force reduction measured at the end of the exercise and expressed as percent of onset value (**c**) and total amount of force produced during the whole exercise (**d**). Data are means ± SEM. * Significantly different from PBS.

Figure 5: Gastrocnemius muscle specific force-generating capacity. Specific force produced throughout the 6-min in vivo fatiguing exercise performed simultaneously to the dynamic ^{31}P-MRS acquisition after a 8-week treatment with PBS or sActRIIB-Fc (**a**). Treatment with sActRIIB-Fc did affect neither maximal specific force (**b**) nor the total amount of specific force produced during the whole exercise (**c**). Data are means ± SEM. * Significantly different from PBS.

Figure 6: Dynamic and noninvasive investigation of gastrocnemius muscle bioenergetics using in vivo ^{31}P-MRS. In vivo changes in gastrocnemius muscle [PCr] (**a**), [P_i] (**b**), [ATP] (**c**) and pH (**d**) throughout the 6-min fatiguing exercise and during the following 15-min recovery period. For each panel, the first time point (t = 0) indicates the basal value. Data are means ± SEM.

Figure 7: Metabolic fluxes and ATP cost of contraction. Oxidative (**a**), anaerobic (**b**) and total (**c**) ATP production, relative contributions of oxidative and anaerobic processes to total ATP production (**d**) and total ATP cost of contraction (**e**) calculated over the in vivo fatiguing exercise after 8-week treatment with PBS or sActRIIB-Fc. Data are means ± SEM.

Figure 1

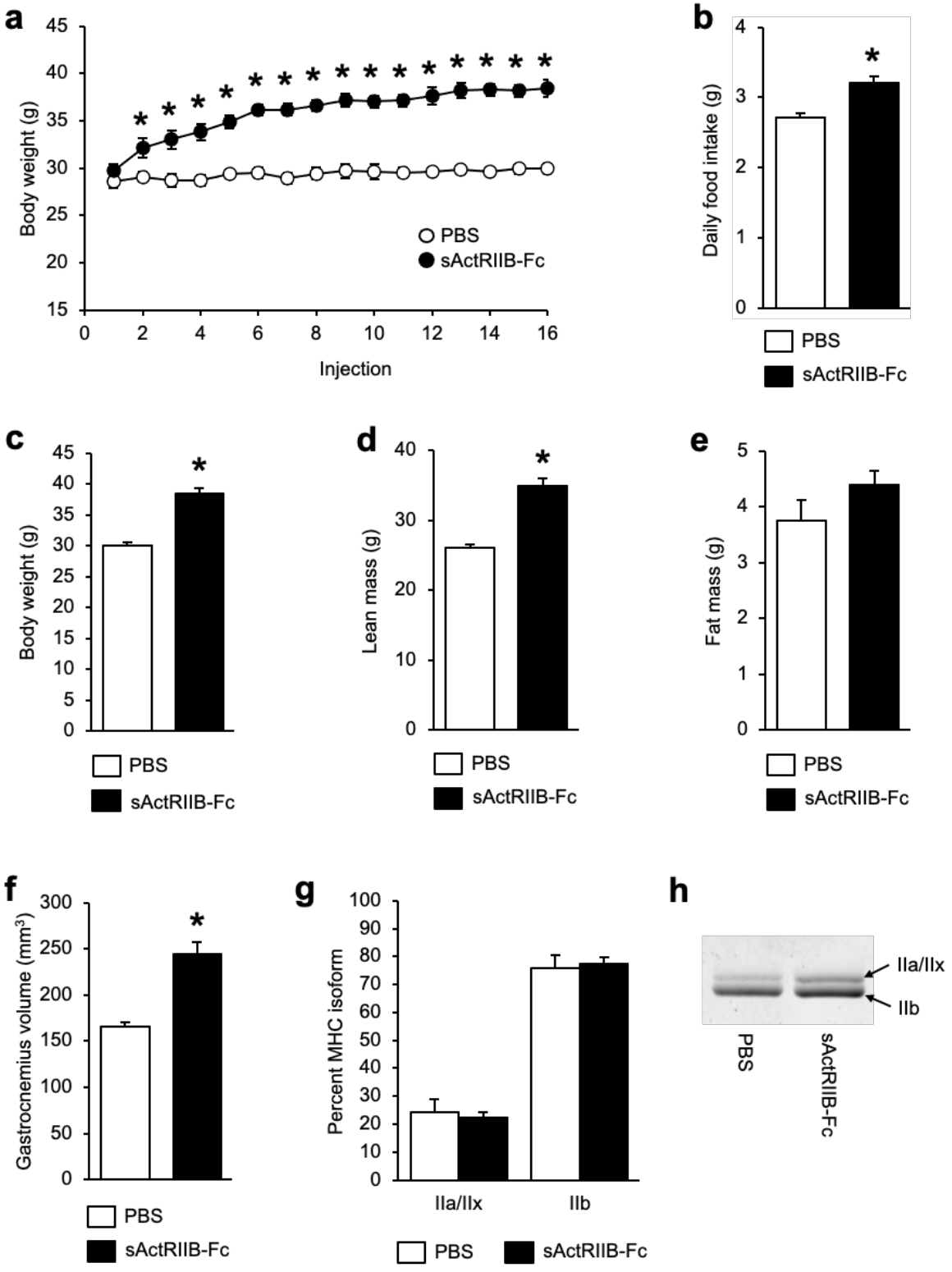
a
Body weight (g)
Injection
PBS
sActRIIB-Fc
b
Daily food intake (g)
PBS
sActRIIB-Fc
c
Body weight (g)
PBS
sActRIIB-Fc
d
Lean mass (g)
PBS
sActRIIB-Fc
e
Fat mass (g)
PBS
sActRIIB-Fc
f
Gastrocnemius volume (mm3)
PBS
sActRIIB-Fc
g
Percent MHC isoform
IIa/IIx
IIb
PBS
sActRIIB-Fc
h
IIa/IIx
IIb
PBS
sActRIIB-Fc

Figure 2

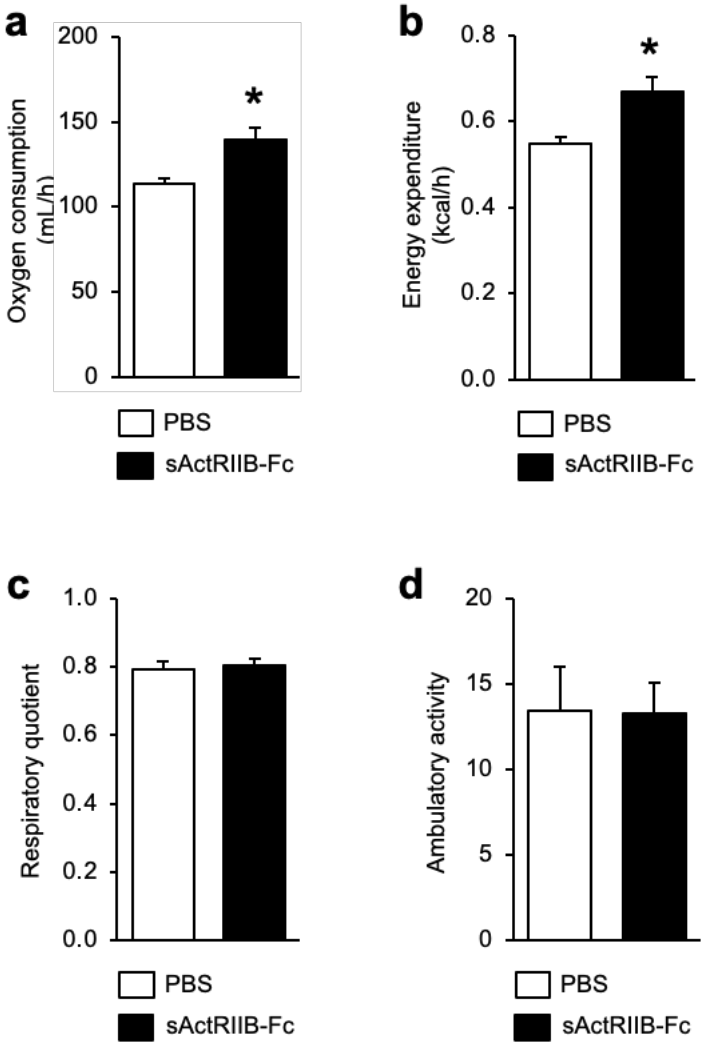
a
Oxygen consumption (mL/h)
200
150
100
50
0
*
PBS
sActRIIB-Fc
b
Energy expenditure (kcal/h)
0.8
0.6
0.4
0.2
0.0
*
PBS
sActRIIB-Fc
c
Respiratory quotient
1.0
0.8
0.6
0.4
0.2
0.0
PBS
sActRIIB-Fc
d
Ambulatory activity
20
15
10
5
0
PBS
sActRIIB-Fc

Figure 3

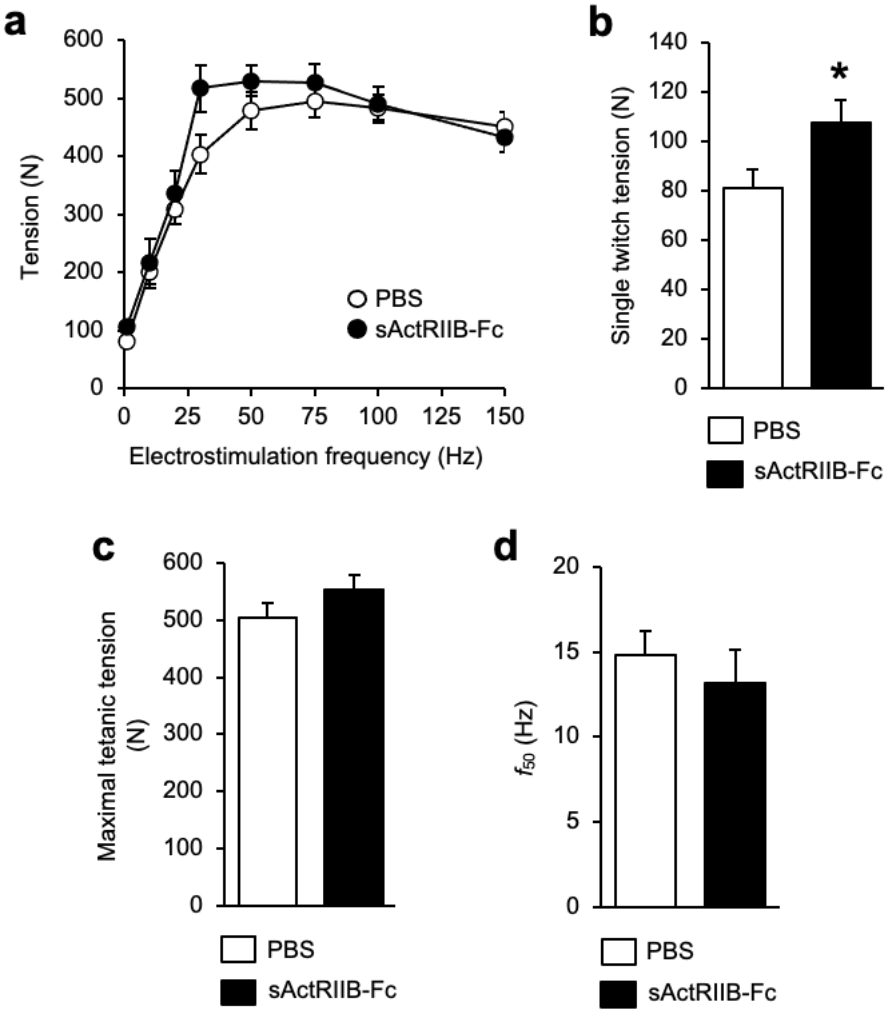
a
Tension (N)
600
500
400
300
200
100
0
0
25
50
75
100
125
150
Electrostimulation frequency (Hz)
PBS
sActRIIB-Fc
b
Single twitch tension (N)
140
120
100
80
60
40
20
0
*
PBS
sActRIIB-Fc
c
Maximal tetanic tension (N)
600
500
400
300
200
100
0
PBS
sActRIIB-Fc
d
f_{50} (Hz)
20
15
10
5
0
PBS
sActRIIB-Fc

Figure 4

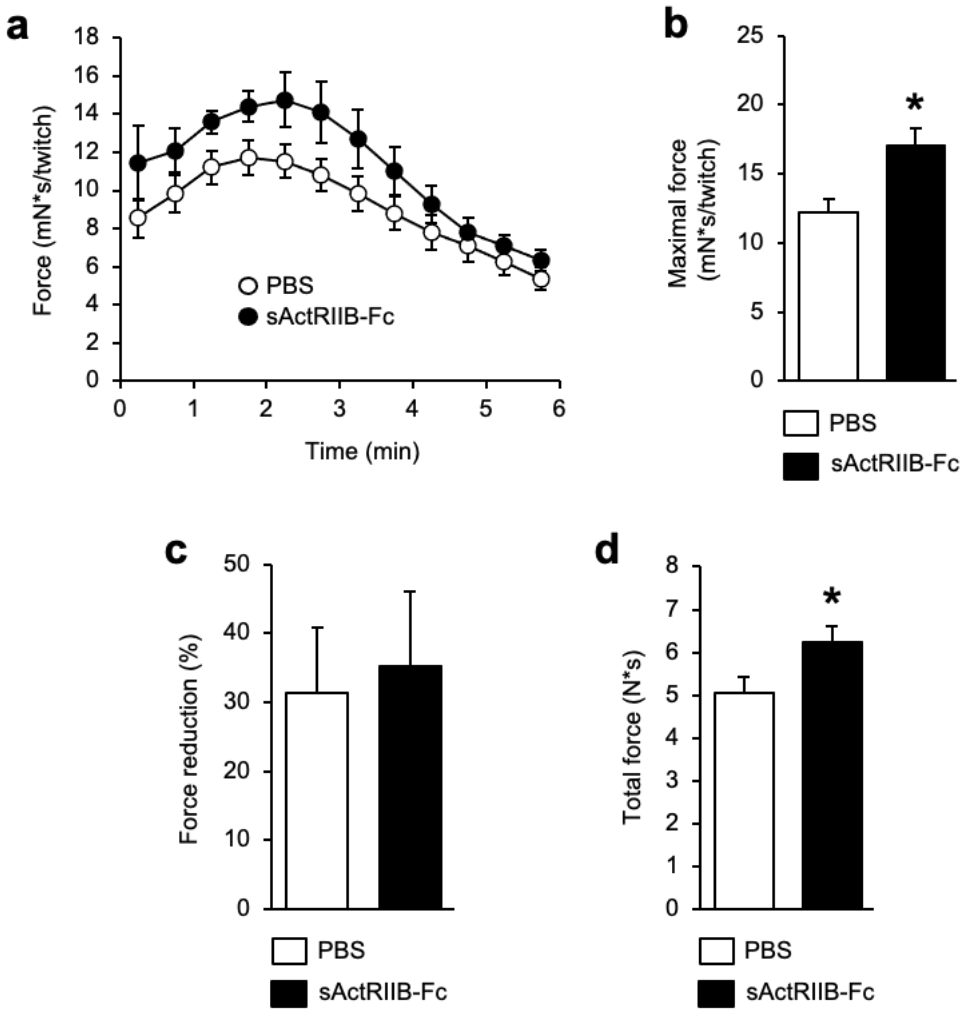
a
Force (mN*s/twitch)
Time (min)
PBS
sActRIIB-Fc
b
Maximal force (mN*s/twitch)
*
PBS
sActRIIB-Fc
c
Force reduction (%)
PBS
sActRIIB-Fc
d
Total force (N*s)
*
PBS
sActRIIB-Fc

Figure 5

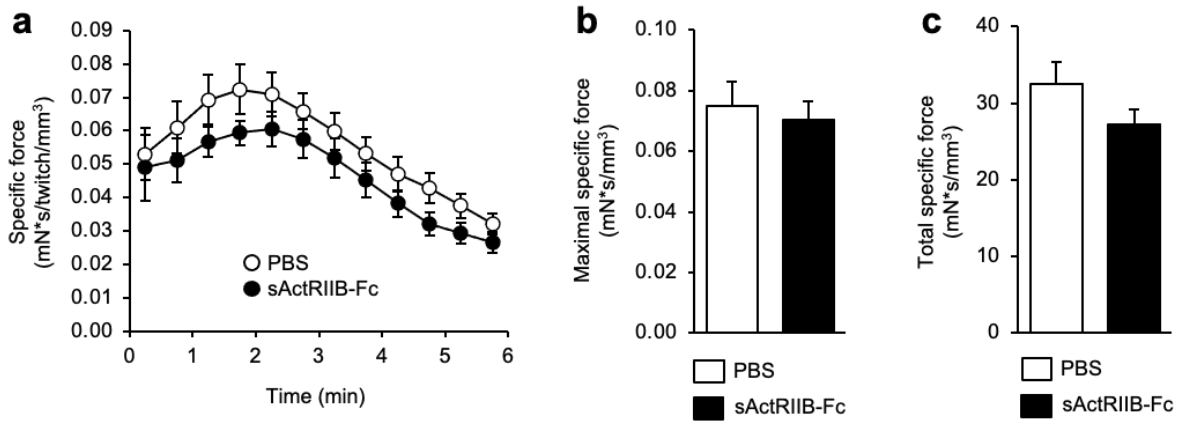
a
Specific force (mN*s/twitch/mm3)
0.09
0.08
0.07
0.06
0.05
0.04
0.03
0.02
0.01
0.00
0
1
2
3
4
5
6
Time (min)
PBS
sActRIIB-Fc
b
Maximal specific force (mN*s/mm3)
0.10
0.08
0.06
0.04
0.02
0.00
PBS
sActRIIB-Fc
c
Total specific force (mN*s/mm3)
40
30
20
10
0
PBS
sActRIIB-Fc

Figure 6

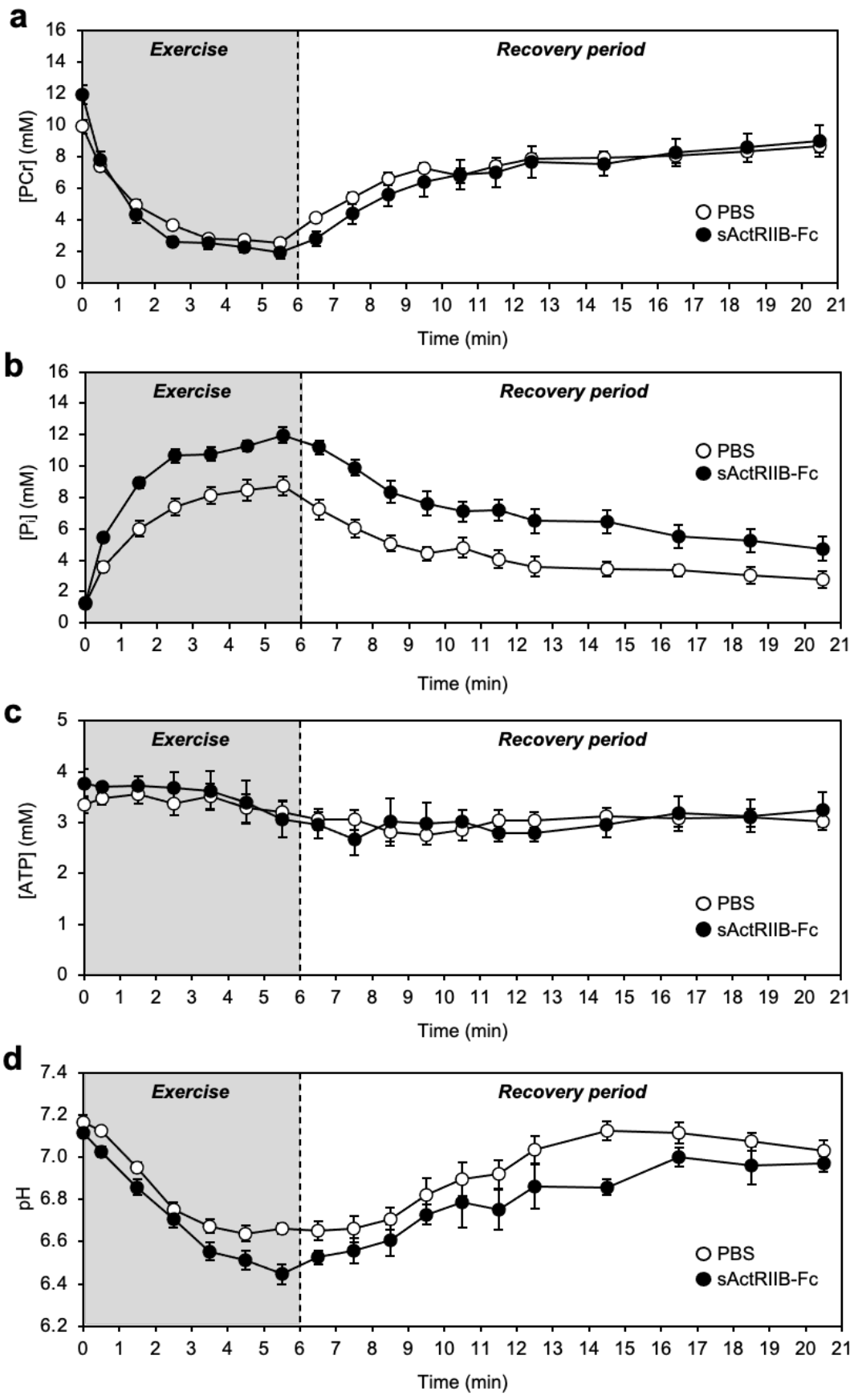
a
Exercise
Recovery period
[PCr] (mM)
PBS
sActRIIB-Fc
Time (min)
b
Exercise
Recovery period
[Pi] (mM)
PBS
sActRIIB-Fc
Time (min)
c
Exercise
Recovery period
[ATP] (mM)
PBS
sActRIIB-Fc
Time (min)
d
Exercise
Recovery period
pH
PBS
sActRIIB-Fc
Time (min)

Figure 7

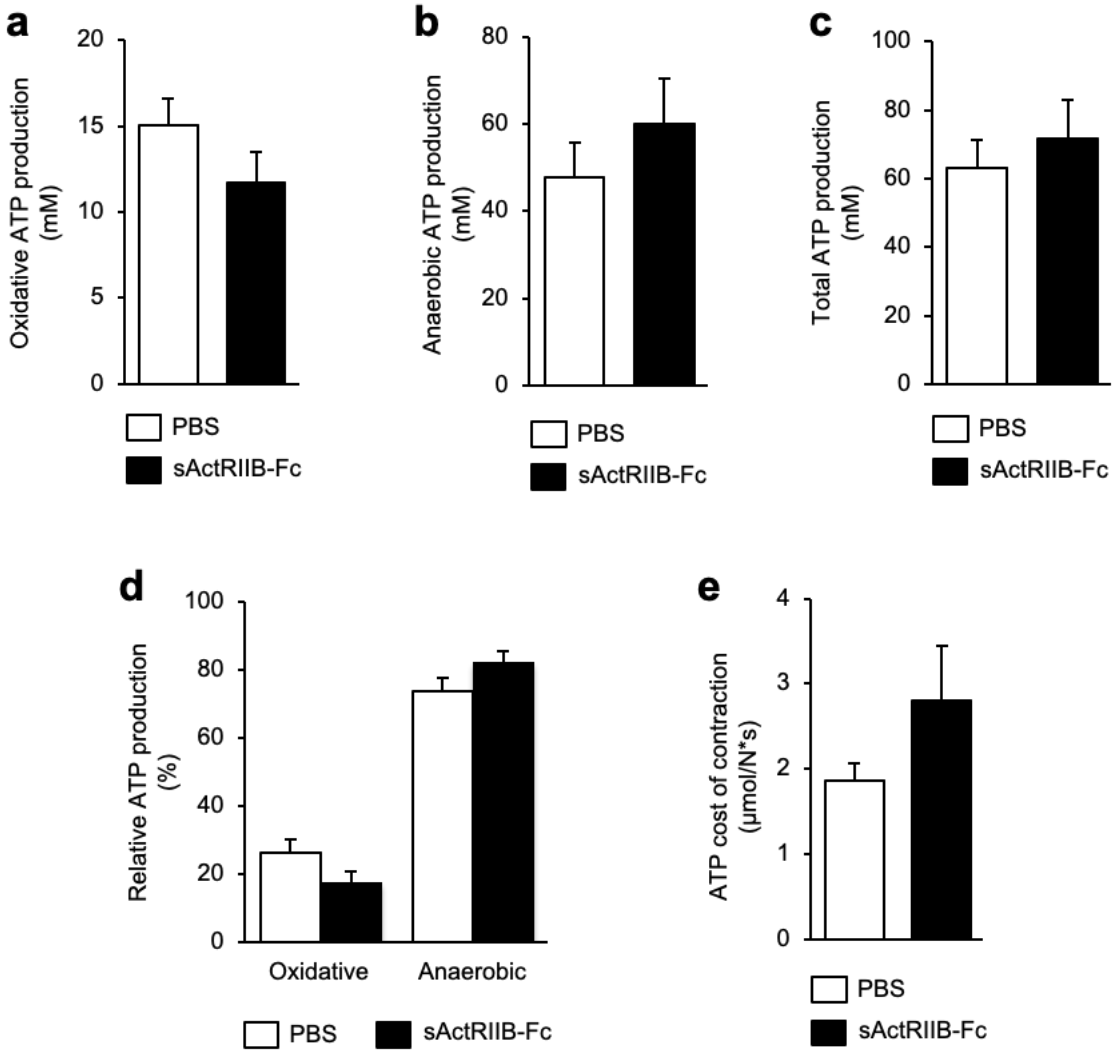
a
Oxidative ATP production (mM)
20
15
10
5
0
PBS
sActRIIB-Fc
b
Anaerobic ATP production (mM)
80
60
40
20
0
PBS
sActRIIB-Fc
c
Total ATP production (mM)
100
80
60
40
20
0
PBS
sActRIIB-Fc
d
Relative ATP production (%)
100
80
60
40
20
0
Oxidative
Anaerobic
PBS
sActRIIB-Fc
e
ATP cost of contraction (µmol/N*s)
4
3
2
1
0
PBS
sActRIIB-Fc